International Journal of Materials Science and Applications
2024, Vol. 13, No. 4, pp. 61-70
https://doi.org/10.11648/j.ijmsa.20241304.11

Research Article

Influence of Temperature on Creep Resistance, Structural and Electrical Characteristics of S9Z1 Eutectic Alloys

Gobran Naji Ali[1, 2], **Mohammed Saleh Nasser Al-Salmi**[2, 3, *]

[1]Medical and Human Scinces Department, Al Dhalea University, Al Dhalea, Yemen
[2]YSMO, Yemen Standardization, Metrology & Quality Control Organization, Sana'a, Yemen
[3]Physics Department, Faculty of Applied Science, Thamar University, Thamar, Yemen

Abstract

In the present study, the structural and creep resistance properties of S9Z1 alloys with Cu-addition in concentrations (0.1 and 0.3% Wt.) have been investigated using x-ray diffractions (XRD) and Creep testing machine respectively. The three samples were prepared from high purity 99.99% by melting technique in the Pyrex tubs with $CaCl_2$ to invaded the oxidation. The obtained samples were rolled drawn (cold rolling) into two groups. The first group was as wires for the creep resistance testing. The second group was as small sheets for structural investigations. Patterns of XRD showed that the S9Z1 alloy was primarily composed of two phases; a body centered tetragonal β-Sn matrix phase, and a secondary phase of hexagonal Zn. while with addition Cu (0.1 and 0.3% Wt.) to S9Z1 Alloys the results showed new peaks in the ternary compositions, such as Cu_6Sn_5, Cu_5Zn_8, phases respectively. The average of particle size (D) of β-Sn matrix was decreased with increasing Cu -adding, whereas the dislocation density (δ) increased with increasing addition. Creep properties of S9Z1, S9Z2 and 3 Alloys were examined at different temperatures (25, 40 and 80 ℃) under two constant loads (σ= 18.7 and 24.94 MPa). The creep behaviors of ternary alloys were higher than the S9Z1 alloys with all different temperatures under two constant loads. Also, the S9Z3 alloy with all different temperatures and two loads exhibited greatest creep resistance, due to the refinement structure and formation of new IMCs. Values of stress exponent (n) were found to be in the range of 1 to 10.55, for all S9Z2 and 3 alloys respectively. Values of activation energy (Q) of alloys were found to be in the range of 36.48 to 37.49 kJ/mol, for σ = 18.7 Mpa and 27 to 34.8 kJ/mol for σ = 24.94 Mpa for the S9Z1 alloys with Cu addition respectively. At room temperature (25 ℃), the electrical conductivity of the samples was calculated, and its values increased with Cu additions.

Keywords

S9Z-xCu, Lead-Free Alloy, Phases, Cu-Additions, Creep Resistance, Structural Properties, Electrical Conductivity

1. Introduction

Lead-free Sn-Zn solder is available in a range of raw materials and melts at a temperature that is nearly the same as conventional Sn-Pb solder. It is currently a possibility to replace the Sn-Pb solder. Since it satisfies industry requirements for electronics without raising the soldering temperature, Eutectic Solder Sn-9wt%Zn is regarded as one of the greatest and most practical substitutes for Eutectic Solder Sn-37Pb in the field of electronic packaging [1, 2]. Due

*Corresponding author: Mohammedalsalmi99@gmail.com (Mohammed Saleh Nasser Al-Salmi)

Received: 4 July 2024; **Accepted:** 30 July 2024; **Published:** 15 August 2024

to lead's high toxicity and detrimental effects on human health, which are the primary driver of global progress, its use is strictly prohibited [3, 4]. In light of the economic revolution, numerous researchers have carried out numerous tests to produce lead-free solder with the appropriate mechanical qualities, melting point, and low cost. High electrical qualities and performance are now standard. [5, 6]. Sn-Zn alloys are widely used because of their low melting temperature (about 198 ℃), which relates them to the solder alloy Sn-37Pb (183 ℃) [9, 7], and their excellent mechanical properties. Their low cost also motivates them to take on the main challenges in the new development of lead-free solder [8, 9]. Sn-Zn alloys are therefore a good option because of their practical characteristics. In addition to its high wettability and strong ductility, zinc's low cost makes it one of the most significant characteristics in the classification of welding materials. notably influences the establishment of trustworthy solder connections, particularly in low volume applications like electronic services, automated processes, and robotics [10-12]. Only a few substitute alloys based on Sn with other elements are being studied because to the limited melting point window. A viable substitute for Sn-Pb alloy would need to meet not only the temperature criteria but also a variety of metallurgical and mechanical qualities of the original alloy. Scientists have created a wide range of binary Pb-free solder alloys, including Sn-Zn, Sn-Cu, Sn-Ag, Sn-Bi, Sn-Sb, and Sn-In. Between these binary systems, Sn-Zn solder alloys have a number of intriguing characteristics. For example, Sn-9Zn eutectic alloys have a melting point of 198 ℃, which is quite similar to Sn-Pb eutectic alloys' 183 ℃. They also have superior mechanical qualities than traditional Sn-Pb solders Furthermore, according to El-Daly et al [7, 13], Cheng et al. [14], it is inexpensive, nontoxic to humans and the environment, and has a low reflow temperature of 222 ℃. Salesm, [15], B. YAVUZER2020. examined the impact of Cu addition on the Sn-9Zn-1.5Ag solder alloy's transient creep capabilities. The presence of extra intermetallic Cu_5Zn_8 phases during solidification was verified by XRD in two samples. The stress exponent of Sn-9Zn solder was discovered to be around (n = 5.0) by Shrestha et al. [16] during their investigation of the creep qualities of it. Chen et al. [17], Cheng et al. [14], Yu et al. [18] and Al-Salmi et al. [19], have reported that although Sn-Zn solders have good mechanical integrity, their resistance to oxidation and corrosion is low. Consequently, because of its low strength (creep resistance), short shelf life, quick oxidation, and micro void formation, Sn-9Zn eutectic solder is challenging to work with. To get over these problems and improve the creep resistance characteristics of lead-free Sn-Zn even more. Although Sn-Zn solders have good mechanical integrity, they are not very resistant to oxidation and corrosion [18, 17, 14].

The Four objectives of this study were to:

a) To create pure Sn-9Zn binary alloys and Sn-9Zn ternary alloys by melting method addition of Cu at values of 0.1 and 0.3 weight percent.
b) To examine the impact of Cu addition on the Sn-9Zn alloy's structural characteristics, such as particle size, dislocation density, lattice parameters, and crystal structure.
c) To examine how Cu addition affects the Sn-9Zn alloy's creep properties (elongation, stress exponents, activation energy, and creep resistance).
d) To examine the impact of Cu) addition on the alloy Sn-9 weight percentage Zn's electrical conductivity characteristics.

2. Experimental Procedure

2.1. Materials and Methods

Table 1. *Alloys' Chemical compositions (all in wt.%).*

S. No.	Alloys	Sn	Zn	Cu
1	S9Z1	91	9	0
2	S9Z2	90.9	9	0.1
3	S9Z3	90.7	9	0.3

Sn-9wt.%Zn, Sn-9wt.%Zn-0.1 wt.% Cu, and Sn-9 wt.%Zn-0.3 wt.% Cu are the solder alloys employed in this work, and they are referred to as S9Z1, S9Z2, and S9Z3, respectively. Table 1. displays the produced alloys' experimental weighted compositions. High purity (99.99%) Sn, Zn, and Cu were used to produce them. All components were melted using an electrical furnace set to 750 ℃ in a Pyrex tub containing $CaCL_2$ (to impede the oxidation of the compositions). They were homogenized by hand agitation at a temperature of 200 ℃ above their melting temperatures. After shaking them to guarantee that the melt was homogenized, they were allowed to gently solidify to room temperature (RT) in order to produce samples that included all of the precipitated phases. The Pyrex container was then shattered in order to extract the sample. The raw alloy materials (as-cast) were rolled into wires of 60 mm in length and one mm in diameter, as well as sheets that were one millimeter thick. Samples of the sheet and wires were polished with grades of silicon paper and then cleaned in a CH_3COCH_3 solution. Following that, the sheets and wires were treated for six hours at 100 ℃, and they were then allowed to cool gradually to room temperature (RT) at a rate of 0.90 ℃ per minute in order to investigate the structural, creep mechanical, and conductivity, respectively.

2.2. Materials Investigation

All of the alloys' chemical compositions Using the XD-2 x-ray diffractometer and the CuKα (λ=1.54 Å) NF model with

measurement accuracy of 0.001 ° and scanning radius of 180 mm, China (in the Yemeni Geological Survey and Minerals Resources Board, YGSMRB), the structural properties of the prepared alloys have been investigated. The XD2 features a minimum step size of 0.00025 °, runs at 36 kV and 20 mA, and has mechanical repeatability that exceeds 0.0006 °. n wt.%). The X-ray tube's focus measurements are 1.0×10^2 mm^2. Using a computerized vertical tensile approach, the tensile creep tests were conducted on all samples at various temperatures (25, 40, and 80˚C) with constant loads (18.7 and 24.94) MPa. Using a simple circuit (DC) of Ohms law, electrical resistance and conductivity were measured.

3. Results and Discussion

3.1. Structural Analysis

Figure 1 exhibits the diffraction patterns observed for each of the three alloys. Drawing from Figure 1a. These patterns clearly show two phases: a secondary phase of hexagonal Zn and a body-centered tetragonal β-Sn matrix phase. There are more Tin Peaks than Zinc Peaks. Because tin is approximately nine times more abundant than zinc. The solid solubility of one in the other is relatively limited, and the Sn-Zn phase diagram indicates that there is no interaction between them. Thus, no additional phases of the system, like those in Figure 1a, are anticipated. This concurs with the findings of Salem [15]; El-Daly and Hammad, [20]. Using the search and match function of the measured data with the relevant reference file and the jade6.5 program, the acquired diffraction patterns have been compared with conventional powder diffraction data (pdf). As per the XRD file presented in Table 2. The Joint Committee on Powder Diffraction Standards at the International Center for Diffraction Data (JCPDS-ICDD) attributes the presence of sharp peaks in the diffraction patterns to the crystalline nature of the three samples (S9Z1, S9Z2, and S9Z3 alloys). based on Figure 1b & c. It is evident that the intensity of all Sn peaks is significantly impacted by Cu-content, and Cu-Sn IMC phases are visible, while the peak broadening and intensity of all Zn peaks have changed. The α-Zn phase peak intensities decrease as the Cu content increases; this IMC, Cu_6Sn_5, has a monoclinic structure. The New Cu-Zn IMC phase was depicted in Figure 1b & c. and is the product of a chemical reaction between copper and zinc. Cu_5Zn_8, which has a cubic structure, is this IMC, based on the Cu-Zn phase diagram and S/M process. As can be observed from Figure 1, the density of this compound increases as the Cu-content increases, leading to higher intensity peaks Zn, however, is reduced by the Cu_5Zn_8 compound's production. All of these findings are consistent with El-Daly and Hammad [20, 21] Additionally, a study of the phases and crystal systems resulting from the addition of Cu (0.1 and 0.3 wt%) to the S9Z1 binary alloy revealed that in Table 2. When Cu was added (0.1 and 0.3%) to S9Z1 Alloys, the β-Sn phase peaks increased and the Zn phase peaks decreased, as seen in Figure 1a, b and c. Due to the appearance of IMCs (Cu-Sn) and IMCs (Cu-Zn), which are Cu_6Sn_5 and Cu_5Zn_8, respectively. The IMCs (Cu_6Sn_5) phases for small (0.1%wt) Cu-addition to S9Z1 Alloy were appearance in three peaks at 2θ (30.32 °, 38.621 ° and 58.5 °), but for large (0.3%wt) Cu-addition, the IMCs of (Cu_6Sn_5) phases was appearance in once peak at 2Θ (32.458 °), also the IMCs (Cu_5Zn_8) phases for small (0.1%wt) Cu-addition to Sn-9Zn Alloy was appearance in once peak at 2θ (43.101 ° while, the IMCs of (Cu_5Zn_8) phases are an appearance in three peaks at 2Θ (40.12 °, 42.9 ° and 64.4 °) at 0.3% wt. Also, rustles showed the effect of Cu in to ternary alloys, the IMCs (Cu_5Zn_8) was increased and the IMCs (Cu_6Sn_5) was reduced with increased Cu-addition in Figure 1b and c.

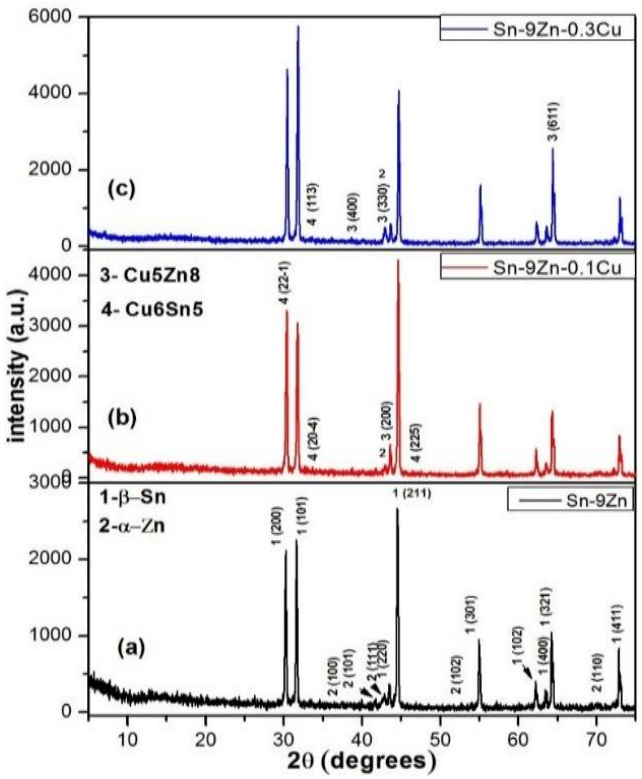

Figure 1. *XRD patterns for all three samples. (a) S9Z1, (b) S9Z2 and (c) S9Z3.*

Table 2. *Three compositions: phases, crystal systems, and PDF Reverence.*

S. wt%	Phases	peaks	Crystal system	(JCPDS-ICDD)Re.
S9Z1	β-Sn	9	Body centered tetragonal	PDF#04-0673
	Zn	5	Hexagonal	PDF#04-0831
S9Z2	β-Sn	9	Body centered tetragonal	PDF#04-0673
	Zn	1	Hexagonal	PDF#04-0831
	Cu_6Sn_5	3	Monoclinic	PDF#45-1488
	Cu_5Zn_8	1	Cubic	PDF#25-1228
S9Z3	β-Sn	9	Body centered tetragonal	PDF#04-0673
	Zn	1	Hexagonal	PDF#04-0831
	Cu_6Sn_5	1	Monoclinic	PDF#45-1488
	Cu_5Zn_8	3	Cubic	PDF#25-1228

Particle sizes of all the as-cast S9Z1, 2 and 3 alloys were determined using the Scherer Formula: [22]

$$D = \frac{0.9\lambda}{\beta Cos\theta} \quad (1)$$

where: B is the broadening of diffraction line measured at half its maximum intensity (radians), t is the diameter of crystal particle, θB is the Bragg angle and λ is the wavelength of x-ray. Table 3. displayed the values for the particle size, lattice distortions, dislocation density (δ), and lattice characteristics. With the addition of Cu, the particle sizes of Zn and β-Sn have dropped, whereas Cu_6Sn_5 has decreased and Cu_5Zn_8 has increased. In the Sn-matrix phase, zinc atoms migrate towards Sn-grain borders, reducing their mobility and preventing grain formation as a result. Various literature sources have discovered and reported this. Zinc has been observed to reduce the β-Sn phase's particle size when added to tin. Reportedly, the same conduct has been [21]. The addition (0.3 wt.% of Cu) cause to shift Cu_6Sn_5 IMC 2θ (30.32 ٩) from (22-1) orientation to (113) orientation at 2θ (32.458 ٩) and the disappearance of the appearance of the three peaks from Cu_6Sn_5 IMC in 0.1 Cu-addition. On the other hand, addition (0.3 wt.% of Cu) cause to shift Cu_5Zn_8 IMC 2θ (43.101 ٩) from (330) orientation to (400), (330) and (611) orientation at 2θ (40.12°, 42.9 °and 64.4 ٩). It is good to mention that the shifted Cu_6Sn_5 IMC and Cu_5Zn_8 IMC cause to slightly increasing lattice distortion (1.79×10^{-3} and 1.61×10^{-3}) in the β-Sn matrix [23] for 0.1 and 0.3 Cu addition to S9Z1 Alloys respectively. The lattice distortion values were calculated according to G. K. Williamson and W. H. Hall. [22]

$$\beta = \left[\frac{1}{D}\right] + 5 \leq \varepsilon^2 \geq^{\frac{1}{2}} Sin\frac{\theta}{\lambda} \quad (2)$$

where D is the size of the crystallite in the β-Sn matrix and ε is a local lattice distortion. About the defects in the S9Z1, 2 and 3 alloys were studied using some factors such as: dislocation density (δ), the results showed that as a function of Cu there is increasing in dislocation density as more Cu added as shown in Figure 2. A slight change has been occurred in (c/a) values from (0.542) to (0.55) due to a lattice expanding in (a) and (c)-axes with Cu additions. Furthermore, Table 3. illustrates how the cell volumes of all as-cast alloys have been rising with Cu additions. Particle size and dislocation density as a function of Cu-addition are displayed in Figure 2.

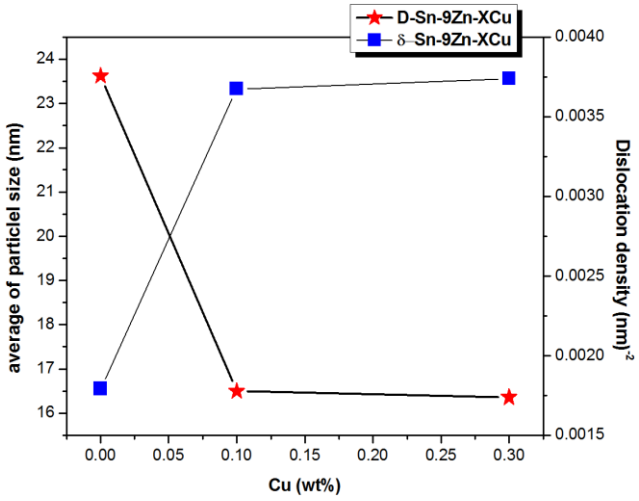

Figure 2. *The particle size and dislocation density as function of Cu-addition.*

Table 3. *The details of the XRD analysis particle size (D), dislocation density (δ) and lattice parameters.*

S. in wt.%	*D* β-Sn (nm)	*D Zn* (nm)	*D* Cu_5Zn_8 (nm)	*D* Cu_6Sn_5 (nm)	(ε) $x10^{-3}$ of β-Sn phase	c/a of β-Sn phase	V $(Å)^3$ of β-Sn phase	δ (nm) $^{(-2)}$ $*10^{-3}$ of β-Sn phase
S9Z1	23.6	16.4	-	-	1.2	0.542	109.14	179
S9Z2	16.5	16.1	3.8	9.7	1.8	0.547	109.7	367
S9Z3	16.4	13.77	14.7	3.5	1.6	0.55	110.7	374

3.2. Creep Properties Strain-Time

For S9Z1, 2 and 3, the creep strain-time curves were displayed in Figure 3a, b, c, d, e, and f, respectively. Following annealing at 100 ℃ and testing at 25 ℃, 40 ℃, and 80°C under two distinct constant stresses (σ = 18.7 and 24.94 MPa), the samples were examined. As seen from the Figure 3a, b, c, d, e, and f respectively, S9Z1 alloy at (T=25 ℃, 40 ℃ and 80 ℃) for loads (σ = 18.7 and 24.94 MPa) respectively, which showed lowest creep resistance, appeared on all the three stages of creep at (σ = 18.7 and 24.94 MPa) with (T=25 ℃, 40 ℃ and 80 ℃) whereas other at (T=25 ℃) for all loads alloys were still in primary creep stage and the steady state creep stage. It can be observed that the S9Z3 and S9Z2 Alloys have greater creep resistance than S9Z1 at all temperatures and under constant loads because of the refinement structure and formation of new IMCs in these as-cast alloys. This is similar to the earlier case, where the stress and temperature (σ = 18.7 and 24.94 MPa) and the temperature (T = 25 ℃, 40 ℃, and 80 ℃, respectively) showed greater creep resistance (low strain rate). Cu_5Zn_8 and Cu_6Sn_5 IMC forms in ternary alloys have the potential to more effectively impede dislocation movement and result in an alloy with a lower creep rate. The S9Z1 alloy exhibits similar behaviours when Cu is added, which rustles agree with D'Souza et al [24].

Using the following equation, the elongation (El.%) for each sample was determined:

$$EL.\% = Strain \times 100 \quad (3)$$

Table 4 lists the elongation for each of the three alloys, which was computed using the data in Figure 3a, b, c, d, e, and f. Additionally, Figure 4 displays the El.% plots. When compared to the EL.% of S9Z2 and S9Z3 at the same load, Figure 4 shows that the EL.% of S9Z1 is increasing at different temperatures (T= 25 ℃, 40 ℃, and 80 ℃) under 18.7 and 24.94 MPa. Conversely, when compared to the eutectic S9Z1 and S9Z3 alloys, the S9Z2 alloy exhibits the longest elongation at T=40 ℃ and 24.94 MPa load.

The creep rate

$$\dot{\varepsilon} = (\partial\varepsilon/\partial t) \quad (4)$$

of the S9Z1, 2 and 3 alloys was determined by looking at the slope of the creep strain-time curves displayed in Figure 3a, b, c, d, e, and f. The values of $(\dot{(\varepsilon)})$ for the three alloys were listed in Table 5 and plotted in Figure 5, which illustrates how the secondary creep rate ($\dot{\varepsilon}$) decreases as the creep life increases at this stage at various temperatures and loads.

Table 4. *Three samples' varying elongations with Cu addition.*

S.	EL.%					
	18.7 MPa			24.94 MPa		
Tem.	25 ℃	40 ℃	80 ℃	25 ℃	40 ℃	80 ℃
S9Z1	4.92	7.45	16..74	11.38	26.39	16.55
S9Z2	3.94	6.64	14.1	5.04	27.62	15.26
S9Z3	2.83	3.26	5.72	3.07	8	7.26

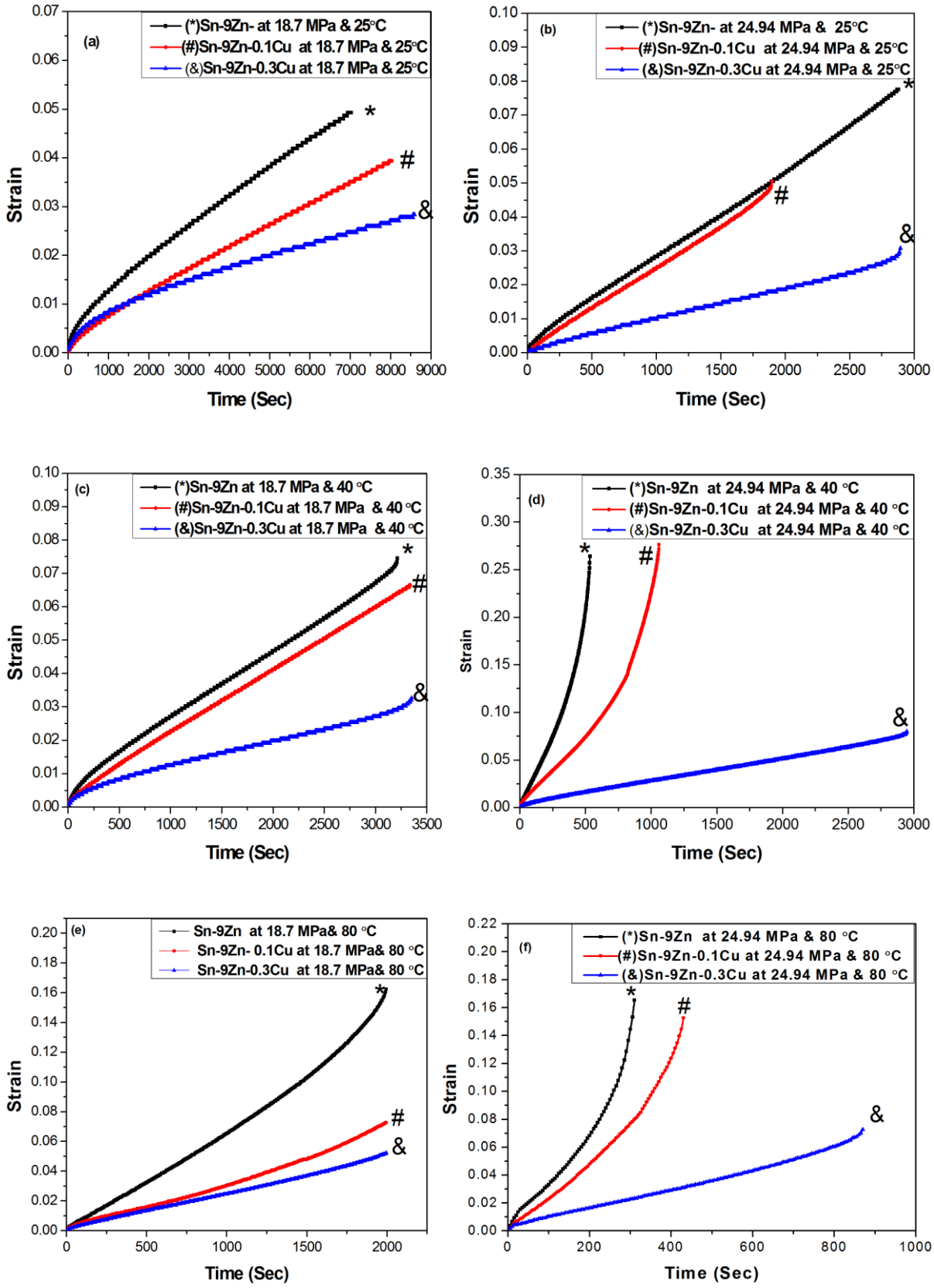

Figure 3. *Creep strain-time curves for Sn-9Zn-xCu at.*

a) T=25℃ &18.7 MPa, b) T=25℃ & 24.94MPa, C) T=40℃ &18.7 MPa, d) T=40℃ &24.94 MPa, e) T=80℃ &18.7 MPa and f) T=80℃&18.7 MPa.

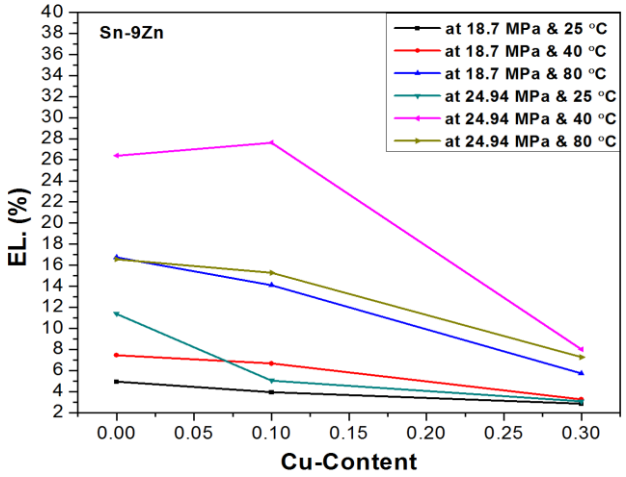

Figure 4. *The elongation for Sn-9Zn-xCu at (T= 25, 40 and 80 ℃) with 18.7 and 24.94 MPa.*

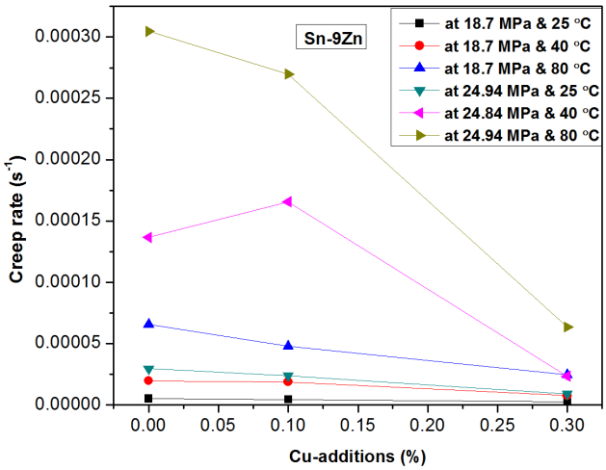

Figure 5. *The creep rate (ε̇) for Sn-9Zn-xCu at (T= 25 ℃, 40 and 80 ℃) with 18.7 and 24.94 MPa.*

The strain rate sensitivity parameter (m=1/n) and stress exponent (n) parameters were calculated by using equation. [25].

$$n = \frac{\partial \mathrm{Ln}(\dot{\epsilon})}{\partial \mathrm{Ln}(\sigma)} \quad (6)$$

The calculated value of n at different temperatures with loads for the tested alloys are listed in the figure 6. From figure 6, the stress exponent values are slightly reduced with high temperature (T= 80 ℃) in all alloys investigated, this reducing is owing to the instability of microstructure at elevated temperatures [13, 19, 24]. The experimental results show that the S9Z1, S9Z2 and S9Z3 alloys have the stress exponents (n); (6, 6.7 & 4), (5.8, 10.55 & 6.1) and (4.46, 6.8, 1) correspond to the testing temperatures (25, 40 and 80) ℃, respectively. The eutectic S9Z2 at temperature (T= 40 ℃) is the particles reinforcement. Whereas, the dislocation movement (climb-creep) controlling mechanism for the all S9Z1, at temperatures (T= (25, 40 and 80) ℃), S9Z2 at temperatures (T= (25 and 80) ℃) and S9Z3 at temperatures (T= (25 and 40) ℃) alloys. While, at temperature (T= 80 ℃) the n value of S9Zalloy revered to the diffusional creep mechanism. The decrease of n-value with 0.3Cu-addition and increasing temperature is a well-known phenomenon that is attributed to the instability of microstructure at elevated temperatures. Softening and dissolution of second phase particles IMCs (Cu_5Zn_8) are possible causes for the observed instability. In general, the enhancement in creep resistance with the addition of 0.1 and 0.3 wt.% of Cu to S9Z1 alloy can be attributed to the interactions of dislocations with the (Cu_5Zn_8 IMC) particles, which hinder the climb of dislocations. Other similar results obtained by the researches of El-Daly, A., et al. [26, 27].

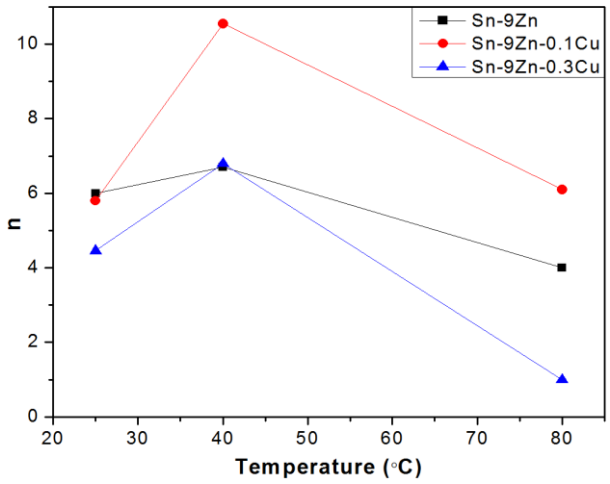

Figure 6. *The stress exponent (n) values at different temperature with Cu-addition.*

Activation energy (Q) of creep is described as the energy barrier that is needed for an atom to move from a high energy location to a lower energy location [25, 28, 29]. The activation energy of steady state creep at constant stresses was calculated using equation.

$$Q = -R\left(\frac{\partial \mathrm{Ln}(\dot{\varepsilon})}{\partial \mathrm{Ln}\left(\frac{1}{T}\right)}\right) \quad (7)$$

Also, the activation energy of steady state creep was calculated from the relation between Ln (Creep rate) and 1000/T at (T=25, 40 and 80 ℃) for S9Z1 eutectic, S9Z2 and S9Z3 alloys under two different applied stresses in the Figure 7a and b. The activation energies for the binary eutectic and ternary alloys have been found to be (Q= 36.48: 34.88: 34.59 kJ mol−1) and (Q= 27: 33.98: 34.1 kJ. mol−1) in the low and high stress, respectively seen Figure 7a and b and are listed in the Table 5. It is clear that the average (Av.) of activation energy for Sn-9Zn binary alloys are small than ternary S9Z2 and S9Z3 alloys in low and high stress, this is consistent with

its high creep resistance and agree with [25-27].

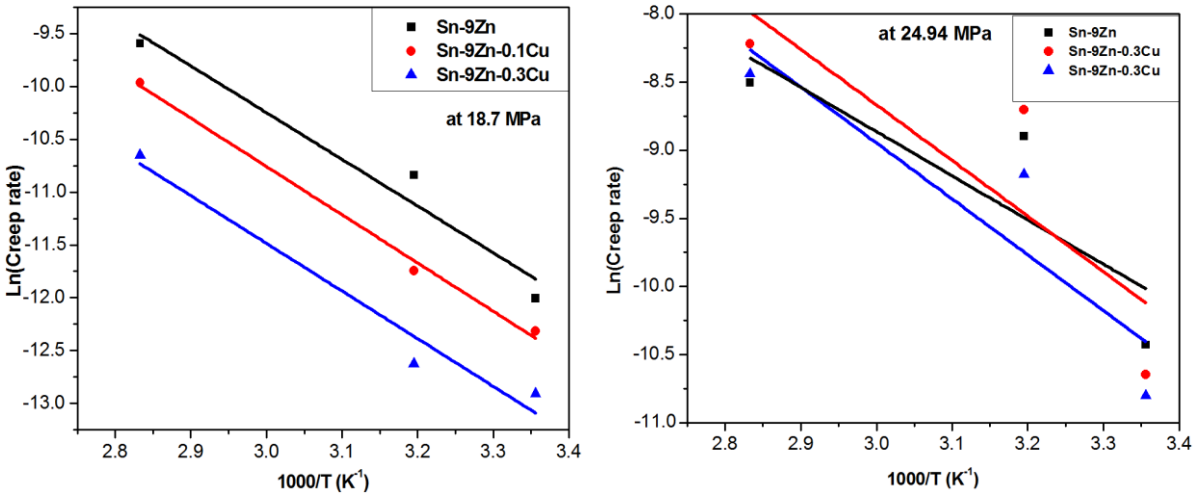

a b

Figure 7. *a. The relation between Ln(ε̇) and 1000/T for S9Z1, 2 and 3 alloys at 18.7 MPa; b. The relation between Ln(ε̇) and 1000/T for S9Z1, 2 and 3 alloys at 24.94 MPa.*

Table 5. *The variation of (Q) of three samples with Cu-addition at different Stress.*

S. in%wt.	Q (KJ/mol)		Av. Q (KJ/mol)
	18.7 MPa	24.94 MPa	
S9Z1	36.48	27	31.74
S9Z2	37.97	33.98	35.98
S9Z3	37.49	34.8	36.15

4. Conductivity and Electrical Resistivity

Regarding electrical properties, electrical resistivity (ρ) and conductivity (σ) were calculated using following equations:

$$\rho = R\frac{A}{l} \text{ and } \sigma = \frac{1}{\rho} \quad (8)$$

respectively, where L is the length of the specimen, R is the ohm resistance and A is the cross-section area. [30, 31]. Figure 8 shows the S9Z1, 2, and 3 alloys' electrical resistivity and conductivity at room temperature (T= 25 ℃). At room temperature (T = 25 ˚C), Table 6 and Figure 8 display the electrical resistivity and conductivity of S9Z1, 2 and 3 alloys. Additions of Cu have generally resulted in an decrease in the ρ values, but an increase in the σ values. Cu_5Zn_8 and Cu_6Sn_5 formation in S9Z1 Alloys with Cu-Additions may be enhanced, which could explain the decreasing and increasing values for ρ and the σ receptively.

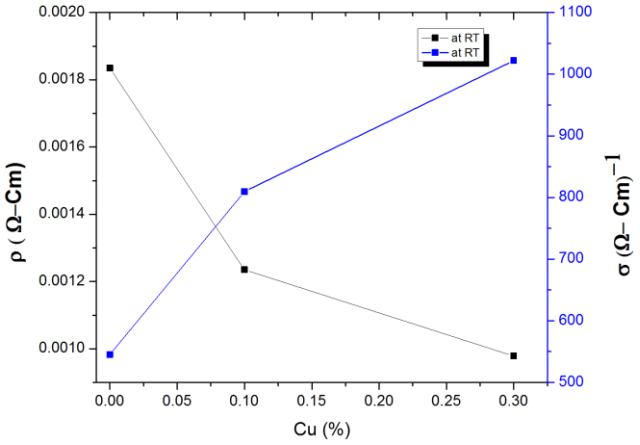

Figure 8. *Electrical resistivity and conductivity behaviour for S9Z1 alloys with Cu additions at T= 25 ℃.*

Table 6. *The (ρ) and (σ) fluctuation at different Stress for three samples with Ag addition.*

S. in Wt.%	ρ (Ω-Cm) * 10^{-3}	σ (Ω-Cm)$^{-1}$
S9Z1	1.83	546.45
S9Z2	1.13	884.96
S9Z3	1.12	892.88

5. Conclusions

The influence of Cu addition in two weight percent concentrations (0.1 and 0.3 wt%) on the structural, mechanical (creep resistance), and conductivity properties of S9Z1 alloys have been examined in this work. The following is a summary of the findings:

According to structural analysis, body-centered tetragonal β-Sn, hexagonal Zn, monoclinic Cu_6Sn_5, and cubic Cu_5Zn_8 phases are formed when Cu is added to Sn-9Zn eutectic alloys.

The creep resistance of S9Z2 and S9Z3, alloys are higher than that of S9Z1 alloy at all different temperature with tow constant loads. Also, S9Z3 alloy exhibited greatest creep resistance (low strain rate), due to the refinement structure and formation of new IMCs in alloys.

The n values referred to the deformation mechanism is dislocation climb for all S9Z1, 2 and 3 alloys, Excepted, at T= 40 ℃ for S9Z2 the creep mechanism is the particles reinforcement and at T= 80 ℃ for S9Z3 alloy the dislocation movement (diffusional creep) controlling mechanism.

In general, increasing of Average (Q) with Cu,-Addition, this is consistent with its high creep resistance. Also, it is noticeable that activation energy decrease with increase the applied stress which means that activation energy depends strongly on applied stress.

The decreasing and increasing for ρ and σ, may be due to enhancing the Cu_6Sn_5 and Cu_5Zn_8 formation in S9Z1 Alloys with Cu-Additions.

Abbreviations

℃	Temperature Percentage " Celsius"
β	Rigid Solution
Sn	Tin
Zn	Zinc
Cu	Copper
XRD	X-Ray Diffraction
FWHM	Full Width at Half Maximum
IMC	Intermetallic Compound
MPa	Mega Pascal
RT	Room Temperature
D	Particle Size
δ	Dislocation Density
JCPDS-ICDD	Joint Committee on Powder Diffraction Standards at the International Center for Diffraction Data

Conflicts of Interest

The authors declare no conflicts of interest.

References

[1] Sharif, A., Y. C. J. J. o. a. Chan, and compounds, Investigation of interfacial reactions between Sn–Zn solder with electrolytic Ni and electroless Ni (P) metallization. 2007. 440(1-2): p. 117-121. http://dx.doi.org/10.1016/j.jallcom.2006.09.020

[2] Billah, M. M., K. M. J. A. M. Shorowordi, and Materials, Effect of micron size Ni particle addition on microstructure, thermal and mechanical properties of Sn-9Zn lead-free solder alloy. 2012. 229: p. 271-275. http://dx.doi.org/10.4028/www.scientific.net/AMM.229-231.271

[3] Olufemi, A. C., et al., Potential health risks of lead exposure from early life through later life: implications for public health education. 2022. 19(23): p. 16006. http://dx.doi.org/10.3390%2Fijerph192316006

[4] Wang, H., et al., Effect of lead exposure from electronic waste on haemoglobin synthesis in children. 2021. 94: p. 911-918. http://link.springer.com/article/10.1007/s00320-020-01619-1

[5] Raabe, D. J. C. r., The materials science behind sustainable metals and alloys. 2023. 123(5): p. 2436-2608. http://dx.doi.org/10.1021/acs.chemrev.2c00799

[6] Mohamed, H., et al., Evaluation of the microstructure, thermal, and mechanical characteristics of Sn-9Zn reinforced with Ni and ZrO_2 nanoparticles via vacuum melting process. 2023. 98(10): p. 105912. http://dx.doi.org/101088/1402-4896/acf3af

[7] El-Daly, A., et al., Thermal and mechanical properties of Sn–Zn–Bi lead-free solder alloys. 2009. 484(1-2): p. 134-142. http://dx.doi.org/10.1016/j.jallcom.2009.04.108

[8] Negm, S. E. A., A. A. Moghny, and S. I. J. R. i. M. Ahmad, Investigation of thermal and mechanical properties of Sn-Zn and Sn-Zn-Bi near-eutectic solder alloys. 2022. 15: p. 100316. http://dx.doi.org/10.1016/j.rinma.2022.100316

[9] Lin, P., et al., Effect mechanism of Ag and Bi elements on the corrosion process in Sn–9Zn–1Ag and Sn–9Zn–3Bi solders. 2019. 6(11): p. 1165a2. http://dx.doi.org/10.1088/2053-1591/ab2663

[10] Zhang, L., et al., Development of Sn–Zn lead-free solders bearing alloying elements. 2010. 21: p. 1-15. http://dx.doi.org/10.1007/s10854-009-0014-1

[11] Liu, S., et al., Present status of Sn–Zn lead-free solders bearing alloying elements. 2015. 26: p. 4389-4411. http://dx.doi.org/10.1007/s10854-014-2659-7

[12] Gerhátová, Ž., et al., Microstructure and corrosion behavior of Sn–Zn alloys. 2022. 15(20): p. 7210. http://doi.org/10.3390/ma15207210

[13] El-Daly, A., Y. Swilem, and A. Hammad, Creep properties of Sn–Sb based lead-free solder alloys. Journal of Alloys and Compounds, 2009. 471(1-2): p. 98-104. http://dx.doi.org/10.1016/j.jallcom.2008.03.097

[14] Cheng, S., C.-M. Huang, and M. J. M. R. Pecht, A review of lead-free solders for electronics applications. 2017. 75: p. 77-95. http://dx.doi.org/10.1016/j.microrel.2017.06.016

[15] Salem, M. Y. J. A. J. o. N. S. and Applications, Effect of small addition Indium on transient and steady-state creep characteristics, microstructure and properties of Sn-9Zn lead-free solders. 2018. 51(3): p. 69-86. http://dx.doi.org/10.1016/j.msea.2010.04.078

[16] Shrestha, T., et al., Creep deformation behavior of Sn–Zn solder alloys. 2014. 49: p. 2127-2135. http://dx.doi.org/10.1007/s10853-013-7905-5

[17] Chen, K.-I., et al., Effects of small additions of Ag, Al, and Ga on the structure and properties of the Sn–9Zn eutectic alloy. 2006. 416(1-2): p. 98-105. http://dx.doi.org/10.1016/j.jallcom.2005.08.034

[18] Yu, D., et al., Investigation of interfacial microstructure and wetting property of newly developed Sn–Zn–Cu solders with Cu substrate. 2004. 385(1-2): p. 119-125. http://dx.doi.org/10.1016/j.matdes.2009.10.053

[19] Al-Salmi, M., et al., Silver (Ag) Improvements on The Structural, Creep Resistance and Electrical Conductivity Properties of Eutectic Sn-9Zn Alloys. 2020. 2(3): p. 142-155. http://doi.org/10.56807/buj.v2i3.116

[20] El-Daly, A., A. J. J. o. A. Hammad, and Compounds, Elastic properties and thermal behavior of Sn–Zn based lead-free solder alloys. 2010. 505(2): p. 793-800. http://dx.doi.org/10.1016/j.jallcom.2010.06.142

[21] El-Daly, A. and A. Hammad, Effects of small addition of Ag and/or Cu on the microstructure and properties of Sn–9Zn lead-free solders. Materials Science and Engineering: A, 2010. 527(20): p. 5212-5219. http://doi.org/10.1016/j.msea.2010.04.078

[22] Williamson, G. and W. J. A. m. Hall, X-ray line broadening from filed aluminium and wolfram. 1953. 1(1): p. 22-31. http://dx.doi.org/10.18280/acsm.450209

[23] Tanaka, M., et al. Improvement in drop shock reliability of Sn-1.2 Ag-0.5 Cu BGA interconnects by Ni addition. in 56th Electronic Components and Technology Conference 2006. 2006. IEEE. http://dx.doi.org/10.1109/ECTC.2006.1645629

[24] D'Souza, R. C., et al., Comparative study on tensile creep behavior of SN-9ZN, SN-0.7 CU and SN-49ZN-1CU solders. 2013. http://dx.doi.org/10.1007/s11664-002-0098-3

[25] Wu, C. M. L and Huang, M, L.. Creep behavior of eutectic Sn-Cu Lead-Free Solder Alloys. Journal of Electronic Materials. 2002. https://doi.org/10.1007/s11664-002-0098-3

[26] El-Daly, A., et al., *The effect of undercooling on the microstructure and tensile properties of hypoeutectic Sn–6.5 Zn–xCu Pb-free solders.* Materials & Design, 2015. 80: p. 152-162. http://doi.org/10.1016/j.matdes.2015.05.016

[27] El-Daly, A., et al., *Design of lead-free candidate alloys for low-temperature soldering applications based on the hypoeutectic Sn–6.5 Zn alloy.* Materials & Design (1980-2015), 2014. 56: p. 594-603. http://dx.doi.org/10.1016/j.matdes.2013.11.064

[28] Chen, Z., Y. Shi, and Z. Xia, *Constitutive relations on creep for SnAgCuRE lead-free solder joints.* Journal of electronic materials, 2004. 33(9): p. 964-971. http://doi.org/10.1007/s11664-004-0023-z

[29] Glazer, J., *Metallurgy of low temperature Pb-free solders for electronic assembly.* International Materials Reviews, 1995. 40(2): p. 65-93. http://doi.org/10.1179/imr.1995.40.2.65

[30] Callister, W. D., et al., *Materials science and engineering: an introduction*. Vol. 7. 2007: John wiley & sons New York.

[31] La Barre, K. A., *The Art and Science of Classification: Phyllis Allen Richmond, 1921-1997.* 2004.